Impact of the catalytic activity of carbon nanotubes in the performance of Li-O$_2$ batteries

Jean Felipe Leal Silva, Gustavo Doubek, Rubens Maciel Filho

Advanced Energy Storage Division – Center for Innovation on New Energies (AES/CINE), School of Chemical Engineering, University of Campinas (UNICAMP). Rua Michel Debrun, s/n, Campinas, SP, Brazil, ZIP code 13083-841.
jefelipe@outlook.com; jefelipe@feq.unicamp.br

The demand for new energy storage technologies has been rising in recent years with the increased adoption of electric vehicles and intermittent renewable electricity sources such as wind and solar power. Among the new energy storage technologies under development, the Li-O$_2$ battery chemistry represents an option with a very high energy density potential. One of the key components of Li-O$_2$ batteries is the O$_2$ electrode in which the discharge product (Li$_2$O$_2$) is deposited. Among the possible materials to be used in the manufacture of these electrodes, carbon nanotubes represent one of the best options: besides high conductivity and the possibility to tailor structures with high porosity, carbon nanotubes present catalytic activity and can be used as support for other catalysts focused on specific electrochemical reactions. This work presents a model of a Li-O$_2$ battery developed to evaluate the impact of catalytic activity on the capacity of the cell. The model considers a generic catalytic activity, which is varied in a range, combined with different current densities to evaluate the impact of power density and reaction rate in the distribution of discharge products in the electrode. Results suggest a strong compromise between power density and energy density because high power density leads to low energy density and vice versa. The relationship between catalytic activity and properties of carbon nanotubes is also discussed considering the use of this material in the manufacturing of electrodes.

1. Introduction

Wind and solar power are expected to increase their market share in the coming years because of their decreasing installation costs. Therefore, owing to their intermittent nature, energy storage solutions must be developed accordingly (Lu et al., 2017). Among energy storage options, batteries represent a versatile solution because they can be installed in modules in almost any location, different from the currently most used energy storage grid-scale technology, which is pumped hydropower (Bragard et al., 2010). However, installation costs for many battery technologies still represent a barrier for their wide adoption, and one of the main factors affecting cost is energy density (Li et al., 2017). In this context, Li-O$_2$ batteries represent an attractive option because of their potentially high energy density (Tan et al., 2017a).

Interest in Li-O$_2$ batteries has been increasing in the last years mainly with experimental works considering different combinations of electrolytes and O$_2$ electrodes (Kwak et al., 2020). The O$_2$ electrode needs to be an inexpensive material with catalytic properties to ensure high energy efficiency and an adequate lifetime. Many materials have been being considered as potential candidates for the final design of Li-O$_2$ batteries because of factors such as manufacturing process, catalytic nature, or porosity (Tan et al., 2017b). However, these assessments of candidate materials, one by one, are not enough to compare their performance in the final design of the battery for commercialization because they are generally normalized by the weight of catalyst and they are not similar in properties. Moreover, the catalytic activity of the O$_2$ electrode needs to be compatible with the electrolyte capacity to transport Li$^+$ and O$_2$ to the reaction site (Wang et al., 2020).

Therefore, this work presents a model of a Li-O$_2$ battery that evaluates the impact of the catalytic activity on the specific capacity after deep discharge. The model consisted of a Li-O$_2$ cell using carbon nanotubes as the O$_2$

electrode because of the possibility to adjust their reactivity by several methods that create defects in their structure (Tan et al., 2012) and because of the electrical properties and potentially low cost of this electrode material (Kim et al., 2018). Results can be used to determine minimum performance requirements for catalysts in general based on the limitations imposed by mass transfer of reacting species in Li-O₂ batteries.

2. Methodology

2.1 Battery model

The Li-O₂ battery model consists of a 1D representation of a battery, as shown in Figure 1. The following conditions were assumed in the model (Sahapatsombut et al., 2013; Tan et al., 2017a): isothermal operation; discharge product is Li₂O₂ (Eq. 1 and 2); electrolyte behaves according to the concentrated solution theory; the pores of the O₂ electrode (Figure 1) are filled with a binary lithium salt in a non-aqueous electrolyte solution; O₂ transport inside the cell occurs exclusively via molecular diffusion in liquid (no gas phase inside the O₂ electrode and no convection).
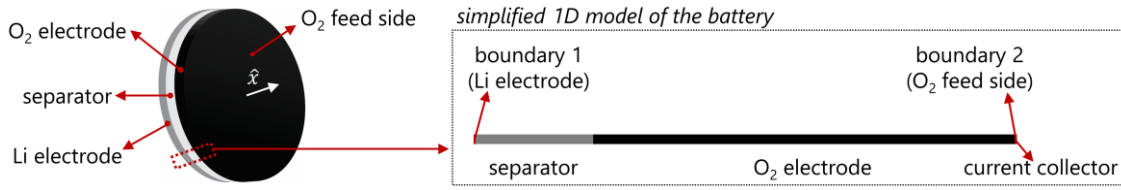

Figure 1: Schematic representation of a Li-O₂ battery and the derived simplified 1D model used in this study

$$Li \rightarrow Li^+ + e^- \qquad\qquad (E^0 = 0.00\ V) \tag{1}$$

$$2\ Li^+ + O_2 + 2e^- \rightarrow Li_2O_2 \qquad\qquad (E^0 = 2.96\ V) \tag{2}$$

The battery is modeled based on the Newman model, which considers solid (discharge products, electrode, etc) and electrolyte solution as a superimposed continuum. The material balance for species i is given by Eq. (3)

$$\partial(\varepsilon C_i)/\partial t = -\nabla \cdot \boldsymbol{N}_i + r_i \tag{3}$$

in which C_i is the concentration, ε is the volume fraction of electrolyte, $\boldsymbol{N}_i$ is the molar flux, and r_i is the production rate. In the absence of convection, the mass transfer for Li⁺ and O₂ is given by Eq. (4) and Eq. (5), respectively:

$$\boldsymbol{N}_{Li} = -D_{Li,eff}\nabla C_{Li} + i_l t_+/F \tag{4}$$

$$\boldsymbol{N}_{O_2} = -D_{O_2,eff}\nabla C_{O_2} \tag{5}$$

in which $D_{Li,eff}$ and $D_{O_2,eff}$ are the effective diffusion coefficients for Li⁺ and O₂, t_+ is the transference number of Li⁺, F is Faraday's constant, and i_l is the current density in the liquid solution, given by Eq. (6) for a binary electrolyte in a Li-O₂ cell:

$$\boldsymbol{i}_l = -\kappa_{eff}\nabla\phi_l - 2RT\kappa_{eff}/F\ (t_+ - 1) + (1 + \partial\ln(f)/\partial\ln(C_{Li}))\nabla\ln(C_{Li}) \tag{6}$$

in which κ_{eff} is the effective ionic conductivity, ϕ_l is the electrolyte potential, R is the universal gas constant, T is the temperature, and f is the activity coefficient of the Li salt. The term $\partial\ln(f)/\partial\ln(C_{Li})$, which is the activity dependence, was fixed at -1.03 (Sahapatsombut et al., 2013). The current density in the O₂ electrode is:

$$i_s = -\sigma_{eff}\nabla\phi_s \tag{7}$$

in which σ_{eff} is the effective conductivity in the electrode. These effective parameters depend on the tortuosity and geometry of the system, and they can be obtained via the porosity of the material using the Bruggeman correlation. In the case of particles with a cylindrical shape, such as carbon nanotubes, these corrections are as follows (Tjaden et al., 2016; Yuan et al., 2015):

$$D_{Li,eff} = \varepsilon^2 D_{Li} \tag{8}$$

$$D_{O_2,eff} = \varepsilon^2 D_{O_2} \tag{9}$$

$$\kappa_{eff} = \varepsilon^2 \kappa \tag{10}$$

$$\sigma_{eff} = (1-\varepsilon)^2 \sigma \tag{11}$$

in which D_{Li} is the diffusion coefficient of Li$^+$ in the electrolyte, D_{O_2} is the diffusion coefficient of O$_2$ in the electrolyte, κ is the conductivity of the electrolyte, and σ is the conductivity of the O$_2$ electrode. In the continuum model, charges are conserved between phases, which can be expressed as:

$$\nabla \cdot \boldsymbol{i}_s + \nabla \cdot \boldsymbol{i}_l = 0 \tag{12}$$

$$\nabla \cdot \boldsymbol{i}_s = aj \tag{13}$$

in which a is the specific surface area of pores per unit volume of the electrode and j is the average transfer current density. In this system, Li$_2$O$_2$ is the only discharge product. Therefore, the rate r_i at which Li$_2$O$_2$ is produced, based on stoichiometry and number of transferred electrons in Eq. (1) and (2), is:

$$r_i = -\frac{as}{nF}j, \qquad in\ which\ s = -2, n = 2 \tag{14}$$

in which s is the stoichiometric coefficient for Li$^+$ in Eq. (1), *i.e.*, -2, and n is the number of transferred electrons (2). For the electrochemical reaction at the O$_2$ electrode, the Butler-Volmer model is used:

$$\frac{j_c}{nF} = k_a\big(C_{Li_2O_2,sol}\big)\exp\left(\frac{(1-\beta)nF\eta_c}{RT}\right) - k_c(C_{Li})^2\big(C_{O_2}\big)\exp\left(\frac{-\beta nF\eta_c}{RT}\right) \tag{15}$$

$$\eta_c = \phi_l - \phi_s - \Delta\phi_{film} - E^0 \tag{16}$$

$$\Delta\phi_{film} = j_c R_{film}\varepsilon_{Li_2O_2} \tag{17}$$

in which C_i is the concentration of a species i, k_a is the anodic rate constant, k_c is the cathodic rate constant, β is the symmetry factor (0.5), η_c is the overpotential of the surface at the O$_2$ electrode, $\Delta\phi_{film}$ is the voltage drop across the Li$_2$O$_2$ film, R_{film} is the resistivity across the Li$_2$O$_2$ film, E^0 is the equilibrium potential (Eq. 2), and $\varepsilon_{Li_2O_2}$ is the volume fraction of the discharge product (Li$_2$O$_2$). At the Li electrode, Eq. (18) is used:

$$j_a = i_0\left(\exp\left(\frac{(1-\beta)nF\eta_a}{RT}\right) - \exp\left(\frac{(1-\beta)nF\eta_a}{RT}\right)\right) \tag{18}$$

in which i_0 and η_a are the exchange current density and the surface overpotential, both at the Li electrode. Initially, the discharge product is formed as a solubilized species. Therefore, up to the solubility limit (C_{max,Li_2O_2}), the change in concentration of Li$_2$O$_2$ is given by Eq. (19), and beyond that, it is given by Eq. (20):

$$\frac{\partial(\varepsilon C_{Li_2O_2})}{\partial t} = -\frac{ai_l C_{Li_2O_2}}{2F}, for\ C_{Li_2O_2} < C_{max,Li_2O_2} \tag{19}$$

$$\frac{\partial(C_{s,Li_2O_2})}{\partial t} = \frac{ai_l C_{Li_2O_2}}{2F}, for\ C_{Li_2O_2} \geq C_{max,Li_2O_2} \tag{20}$$

in which $C_{Li_2O_2}$ is the concentration of Li$_2$O$_2$ in the electrolyte, and C_{s,Li_2O_2} is the concentration of solid Li$_2$O$_2$ (which deposits inside the pores of the O$_2$ electrode). As a result of the formation of the discharge product, the volume fraction of the discharge product ($\varepsilon_{Li_2O_2}$) and the active surface area of the O$_2$ electrode (a) change:

$$\varepsilon_{Li_2O_2} = \frac{(C_{s,Li_2O_2} - C_{s,0,Li_2O_2})M_{Li_2O_2}}{\rho_{Li_2O_2}} \tag{21}$$

$$a = a_0\big(1 - \varepsilon_{Li_2O_2}/\varepsilon_0\big)^p \tag{22}$$

in which $C_{s,0,Li_2O_2}$ is the initial concentration of the solid product, $M_{Li_2O_2}$ is the molecular weight of the Li$_2$O$_2$, $\rho_{Li_2O_2}$ is the density of the discharge product, a_0 is the initial surface area, ε_0 is the initial electrode void fraction, and the exponent p is an empirical value: low values indicate high blockage of the surface area (plate-like structures), whereas high values model the formation of coarser structures. A value of $p = 0.5$ has been used, but this value can be adjusted based on experimental validation. The initial surface area can be calculated based on the initial porosity and the average particle radius r_0:

$$a_o = 2\varepsilon_0/r_0 \tag{23}$$

In Eq. (23), the coefficient 2 is used for nanotubes. At boundary 2 (Figure 1), oxygen is available at a partial pressure of p_{O_2}. The concentration of oxygen at the boundary can be estimated using the ideal gas law (Eq. 24), and the saturated concentration of oxygen inside the electrolyte at the boundary can be estimated using a solubility factor H, as described by Eq. (25):

$$C_{O_2,ext} = p_{O_2}/RT \tag{24}$$

$$C_{O_2} = HC_{O_2,ext} \tag{25}$$

2.2 Simulation and analysis

The battery model was implemented in COMSOL Multiphysics 5.6 (2020, COMSOL Inc., Sweden). The simulations were run on a 64-bit Windows 10 Pro with 32 GB of RAM and an Intel Core i5-9600KF. The Li electrode, represented as boundary 1 in the model (Figure 1), was set to a potential of 0 V, and the desired current density was applied at boundary 2 (Figure 1). The cell potential was also read at boundary 2. The simulation of the galvanostatic discharge process ran indefinitely until a cell potential of 2.5 V was reached. The mesh was physics-controlled with extremely fine elements. To evaluate the impact of catalytic activity, k_c was varied in a range of 1×10^{-18} to 1×10^{-15} m^7 s^{-1} mol^{-2} (Sahapatsombut et al., 2013). Three different current densities (i_{app}) were applied in the study (0.5, 2.0, and 3.5 A m^{-2}) to force different situations of mass transport.

Table 1: Parameters used in the simulation of the Li-O$_2$ cell (Fiates et al., 2020; Gittleson et al., 2017; Laurent et al., 2010; Sahapatsombut et al., 2013)

Variable	Value	Variable	Value	Variable	Value
$C_{Li,0}$	1000 mol m^{-3}	i_0	0.965 A m^{-2}	p_{O_2}	0.21 bar
C_{max,Li_2O_2}	0.09 mol m^{-3}	k_a	1.1×10^{-15} m s^{-1}	R_{film}	50 Ω m^2
D_{Li}	2.50×10^{-10} m^2 s^{-1}	κ	1.5 S m^{-1}	ρ_s	1500 kg m^{-3}
D_{O_2}	1.24×10^{-9} m^2 s^{-1}	σ	100 S m^{-1}	r_0	30 nm
E_0	2.96 V	l_{elec}	250 μm	H	0.4
ε	0.9	l_{sep}	50 μm	T	300 K
ε_{sep}	0.5	$M_{Li_2O_2}$	45.881 g mol^{-1}	t_+	0.45

3. Results and Discussion

3.1 Impact of catalytic activity on cell capacity

Figure 2 shows the discharge curve for the Li-O$_2$ cell for four different cathodic rate constants and three different discharge current densities. For lower current densities, the specific capacity of the cell is not affected by the kinetics: at 0.5 A m^{-2}, all cases reported a capacity of about 12000 mAh g^{-1}. Nevertheless, a higher cathodic rate constant yields a discharge plateau at a higher voltage. Therefore, an increase in the cathodic rate constant increases the voltage efficiency and decreases the energy that would be lost because of overpotential. Similar findings were reported in the literature in the comparison of electrodes based on Ketjenblack carbon using CuFe as the catalyst for the oxygen reduction reaction (Ren et al., 2011).
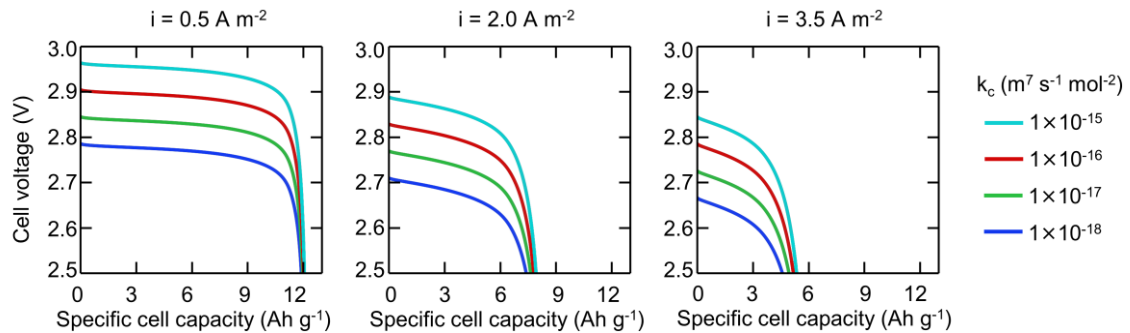

Figure 2: Discharge curve for the Li-O$_2$ cell under different values of k_c and i_{app}

Experimental evaluation of the effect of the catalytic activity on the specific capacity at deep discharge requires reproducibility in electrode manufacturing, which is still challenging (Ren et al., 2011). Nevertheless, according

to this battery model, this effect becomes more evident at larger current densities, though the difference is small. At a current density of 3.5 A m^{-2}, a k_c of 1×10^{-18} m^7 s^{-1} mol^{-2} yields a specific capacity of 4616 mAh g^{-1}, whereas a k_c of 1×10^{-15} m^7 s^{-1} mol^{-2} yields a capacity of 5347 mAh g^{-1} (an increase of 16%). However, at this current density, the voltage drops too fast and compromises cell efficiency. Therefore, the main benefit of increasing the cathodic rate constant is the decrease in cell overpotential.

3.2 Impact of catalytic activity on the distribution of discharge product

Figure 3 presents the combined effect of the cathodic rate constant and applied current density on the porosity (void fraction) of the electrode as a function of the dimensionless length of the electrode. As the discharge progresses, at a low current density, the discharge product becomes well distributed throughout the O$_2$ electrode independently of the cathodic rate constant. On the other hand, at a high current density (3.5 A m^{-2}), because of the sluggish O$_2$ mass transport, the O$_2$ supply decreases, thus increasing the cell overpotential. In this case, a higher cathodic rate constant decreases the cell overpotential, which allows the discharge process to go further, thus leading to an increased cell capacity. In this case, a major part of the discharge product accumulates at the end of the electrode facing the O$_2$ feed side because of limitations in O$_2$ mass transport.

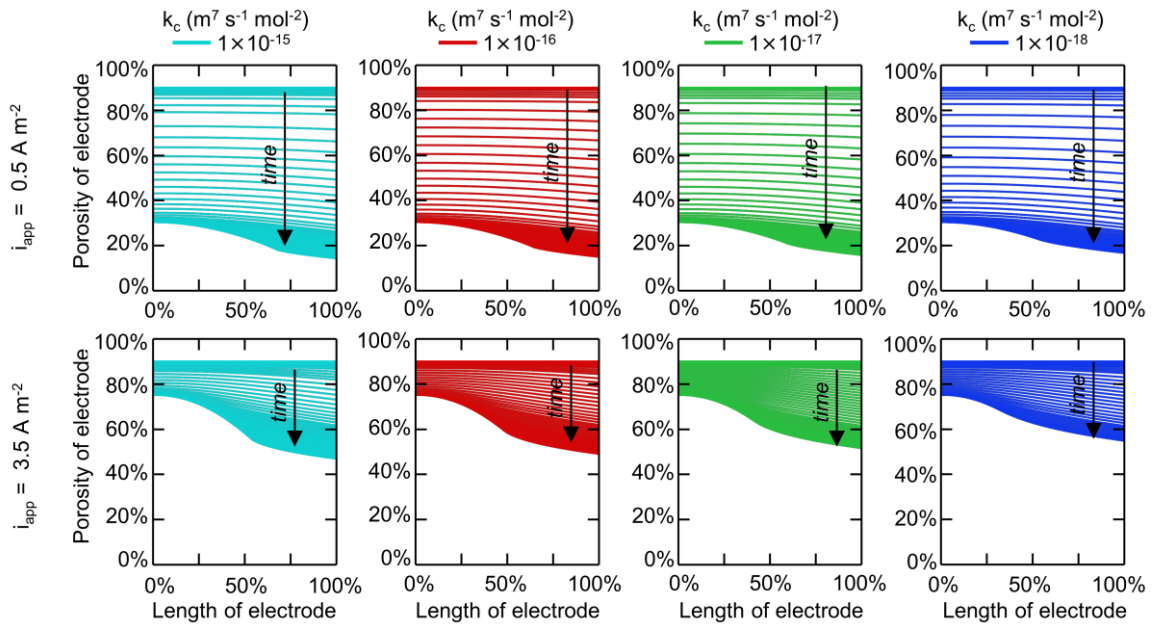*Figure 3: Evolution of porosity as a function of the dimensionless length (0%: separator side, 100%: O$_2$ feed side) of the O$_2$ electrode with time for different values of k_c and i_{app}*

Increased cell capacity at high current density as a consequence of increased catalytic activity has been shown previously (Hou et al., 2020), and it was connected to the achieved decrease in cell overpotential as well. Based on these findings, adjusting the catalytic activity is fundamental to efficiently use the void volume fraction of the O$_2$ electrode, thus increasing the capacity of Li-O$_2$ cells. Previous literature had indicated the possibility of increasing the cell capacity by using a non-uniform catalyst distribution (Andrei et al., 2010). Such an arrangement is only possible by using layered materials of small dimensions, such as carbon nanotubes. The catalytic activity of carbon nanotubes is adjustable by several treatments, and they can be used as support for other more noble catalysts as well. Therefore, carbon nanotubes represent a very suitable candidate to produce Li-O$_2$ batteries with higher energy efficiency.

4. Conclusion

The development of Li-O$_2$ batteries still requires many improvements in terms of catalysis, and an interesting approach is to evaluate the impact of catalytic activity to better understand its impact on battery performance. Results of the simulation of a Li-O$_2$ cell indicate that an increased cathodic rate constant decreases the cell overpotential. At a small current density, this has little impact on the specific capacity of the cell. Nevertheless, at higher current densities, the decreased cell overpotential allowed by the faster kinetics compensates for the low O$_2$ concentration caused by the combined effect of faster discharge and slow O$_2$ mass transport. Overall,

the results indicate that the cathodic rate constant has little impact on the specific capacity of the Li-O$_2$ cell but a great impact on cell overpotential. Therefore, higher energy density and efficiency can be achieved by using materials with increased catalytic activity. This result highlights the importance of using versatile materials such as carbon nanotubes because of the possibility to adjust their catalytic activity.

Acknowledgments

References

Andrei P., Zheng J. P., Hendrickson M., Plichta E. J., 2010, Some Possible Approaches for Improving the Energy Density of Li-Air Batteries, Journal of The Electrochemical Society, 157(12), A1287.

Bragard M., Soltau N., Thomas S., De Doncker R. W., 2010, The balance of renewable sources and user demands in grids: Power electronics for modular battery energy storage systems, IEEE Transactions on Power Electronics, 25(12), 3049–3056.

Fiates J., Zhang Y., Franco L. F. M., Maginn E. J., Doubek G., 2020, Impact of anion shape on Li+solvation and on transport properties for lithium-air batteries: a molecular dynamics study, Physical Chemistry Chemical Physics, 22(28), 15842–15852.

Gittleson F. S., Jones R. E., Ward D. K., Foster M. E., 2017, Oxygen solubility and transport in Li–air battery electrolytes: establishing criteria and strategies for electrolyte design, Energy Environmental Science, 10(5), 1167–1179.

Hou Z., Shu C., Hei P., Yang T., Zheng R., Ran Z., Long, J., 2020, A 3D free-standing Co doped Ni$_2$P nanowire oxygen electrode for stable and long-life lithium–oxygen batteries, Nanoscale, 12, 6785-6794

Kim J. H., Hwang J. Y., Hwang H. R., Kim H. S., Lee J. H., Seo J. W., Shin U. S., Lee S. H., 2018, Simple and cost-effective method of highly conductive and elastic carbon nanotube/polydimethylsiloxane composite for wearable electronics, Scientific Reports, 8(1), 54853.

Kwak, W. J., Rosy, Sharon D., Xia C., Kim H., Johnson L. R., Bruce P. G., Nazar L. F., Sun Y. K., Frimer A. A., Noked M., Freunberger S. A., Aurbach D., 2020, Lithium-Oxygen Batteries and Related Systems: Potential, Status, and Future, Chemical Reviews, 120, 14, 6626–6683.

Laurent C., Flahaut E., Peigney A., 2010, The weight and density of carbon nanotubes versus the number of walls and diameter, Carbon, 48, 10, 2994–2996.

Li J., Du Z., Ruther R. E., An S. J., David L. A., Hays K., Wood M., Phillip N. D., Sheng Y., Mao C., Kalnaus S., Daniel C., Wood D. L., 2017, Toward Low-Cost, High-Energy Density, and High-Power Density Lithium-Ion Batteries, JOM, 69, 9, 1484–1496.

Lu J., Li R., Wang J., 2017, Effect of Collaborative Utilization of Energy Storage and Wind Power on Wind Power Grid-connected and Carbon Emission, Chemical Engineering Transactions, 62, 1117-1122.

Ren X., Zhang S. S., Tran D. T., Read, J., 2011, Oxygen reduction reaction catalyst on lithium/air battery discharge performance, Journal of Materials Chemistry, 21, 10118-10125

Sahapatsombut U., Cheng H., Scott K., 2013, Modelling the micro–macro homogeneous cycling behaviour of a lithium–air battery, Journal of Power Sources, 227, 243–253.

Tan C. W., Tan K. H., Ong Y. T., Mohamed A. R., Zein S. H. S., Tan S. H., 2012, Energy and environmental applications of carbon nanotubes, Environmental Chemistry Letters, 10, 3, 265–273.

Tan P., Kong W., Shao Z., Liu M., N, M., 2017a, Advances in modeling and simulation of Li–air batteries, Progress in Energy and Combustion Science, 62, 155–189.

Tan P., Liu M., Shao Z., Ni M., 2017b, Recent Advances in Perovskite Oxides as Electrode Materials for Nonaqueous Lithium–Oxygen Batteries, Advanced Energy Materials, 7, 13 1602674.

Tjaden B., Cooper S. J., Brett D. J., Kramer D., Shearing P. R., 2016, On the origin and application of the Bruggeman correlation for analysing transport phenomena in electrochemical systems, Current Opinion in Chemical Engineering, 12, 44–51.

Wang F., Li X., Hao X., Tan J., 2020, Review and Recent Advances in Mass Transfer in Positive Electrodes of Aprotic Li-O$_2$ Batteries, ACS Applied Energy Materials, 3(3), 2258–2270.

Yuan J., Yu J.-S., Sundén B., 2015, Review on mechanisms and continuum models of multi-phase transport phenomena in porous structures of non-aqueous Li-Air batteries. Journal of Power Sources, 278, 352–369.